Title

The Parvalbumin/Somatostatin Ratio Is Increased in Pten Mutant Mice and by Human PTEN ASD Alleles

Journal

Cell Reports, 11(6)

ISSN

2639-1856

Authors

Vogt, Daniel
Cho, Kathleen KA
Lee, Anthony T
et al.

Publication Date

2015-05-01

DOI

10.1016/j.celrep.2015.04.019

Peer reviewed

HHS Public Access

Author manuscript

Cell Rep. Author manuscript; available in PMC 2016 May 12.

Published in final edited form as:

Cell Rep. 2015 May 12; 11(6): 944–956. doi:10.1016/j.celrep.2015.04.019.

Parvalbumin/Somatostatin Ratio Is Increased in *Pten* mutant Mice and by Human *PTEN* ASD alleles

Daniel Vogt[1,3], **Kathleen K. A. Cho**[4,5], **Anthony T. Lee**[4,5], **Vikaas S. Sohal**[4,5], and **John L. R. Rubenstein**[1,2,3]

Daniel Vogt: Daniel.Vogt@ucsf.edu; John L. R. Rubenstein: John.Rubenstein@ucsf.edu

[1]Department of Psychiatry, University of California San Francisco, San Francisco, CA 94158, USA

[2]Neuroscience Program, University of California San Francisco, San Francisco, CA 94158, USA

[3]Nina Ireland Laboratory of Developmental Neurobiology, University of California San Francisco, San Francisco, CA 94158, USA

[4]Center for Integrative Neuroscience, University of California San Francisco, San Francisco, CA 94143, USA

[5]Sloan-Swartz Center for Theoretical Neurobiology, University of California San Francisco, San Francisco, CA 94143, USA

Summary

Mutations in the phosphatase *PTEN* are strongly implicated in autism spectrum disorder (ASD). Here we investigate the function of *Pten* in cortical GABAergic neurons using conditional mutagenesis in mice. Loss of *Pten* results in a preferential loss of SST^+ interneurons, that increases the ratio of PV/SST interneurons, ectopic PV^+ projections in layer I, and increases in inhibition onto glutamatergic cortical neurons. *Pten* mutant mice exhibit deficits in social behavior and changes in EEG power. Using MGE transplantation, we test for cell-autonomous functional differences between human *PTEN* wild type (WT) and ASD alleles. The *PTEN* ASD alleles are hypomorphic in regulating cell size and the PV/SST ratio compared to WT *PTEN*. This MGE transplantation/complementation assay is efficient and is generally applicable to functionally test ASD alleles *in vivo*.

Graphical abstract

Author Contributions

DLV, KKAC and ATL performed experiments. All authors conceived experiments and wrote the manuscript.

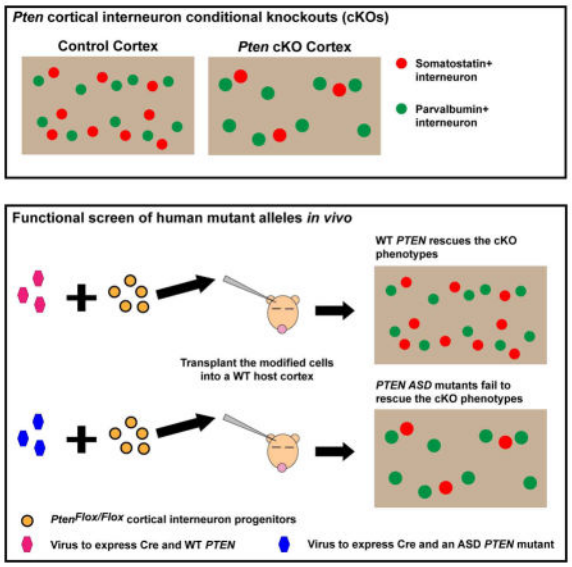

Introduction

Autism spectrum disorder (ASD) is characterized by deficits in language, social interactions and repetitive behaviors. Some forms of ASD may be caused by an imbalance in excitatory/inhibitory (E/I) tone in the brain (Rubenstein and Merzenich, 2003). An increasing number of ASD genetic risk loci are being identified (Murdoch and State, 2013; Tebbenkamp et al., 2014). Recent data from mouse models, including *MeCP2* (Chao et al., 2010), *Scn1a* (Han et al., 2012), *Caspr2* (Peñagarikano et al., 2011), *Caspr4* (Karayannis et al., 2014), *Shank3* and the mouse strain BTBR (Gogolla et al., 2014), showed defects in GABAergic neurons that contribute to ASD phenotypes by altering E/I balance. This balance may be disrupted by altering the relative numbers, functions and/or connectivity between excitatory neurons and inhibitory interneurons.

In the neocortex, glutamatergic excitatory neurons comprise ~70% of all neurons, and GABAergic inhibitory interneurons account for ~30%. The majority of interneurons arise from the medial and caudal ganglionic eminences (MGE and CGE) of the basal ganglia. Immature interneurons tangentially migrate from the MGE to the cortex, then radially migrate into cortical layers (Anderson et al., 1997). As MGE cells mature, they express specific molecular markers of interneuron subtypes, including somatostatin (SST) and parvalbumin (PV) (Wonders and Anderson, 2006). CGE-derived interneurons express vasoactive intestinal peptide (VIP) and Reelin (that lack SST) (Miyoshi et al., 2010). Furthermore, interneuron subgroups project to different cortical layers and synapse within distinct domains of the neocortex (Huang et al., 2007). Thus, perturbations in different interneuron subgroups can lead to E/I imbalance by a variety of mechanisms.

While most ASD genes individually account for <1% of the genetic risk, some genes, including the phosphatase, *PTEN*, are more often mutated in ASD (O'Roak et al., 2012). PTEN inhibits PI3K/Akt-signaling after its activation by receptor tyrosine kinases (RTKs) and other receptors (Bourgeron, 2009; Stiles, 2009). The growth-promoting Akt/mTor

signaling cascade is also a hub for other ASD candidate genes, including *Tsc1&2* (Wiznitzer 2004), and *NF1* (Marui et al., 2004; Mbarek et al., 1999).

Pten is broadly expressed in the developing and adult mouse brain, including in glutamatergic and GABAergic neurons (herein and Ljungberg et al., 2009). *Pten* regulates many developmental processes, including migration (Kölsch et al., 2008), growth and morphogenesis (Kwon et al., 2006), and synaptic dynamics (Fraser et al., 2008; Luikart et al., 2011; Williams et al., 2015). Conditional deletion of *Pten* in excitatory cortical neurons results in macrocephaly, overgrowth of cortical cell bodies (somas), axons and dendrites; and leads to social interaction deficits; some of these features were rescued by pharmacologic inhibition of the mTor pathway (Kwon et al., 2006; Zhou et al., 2009). However, the role of *Pten* and other genes in the Akt/mTor pathway are poorly understood in GABAergic cortical interneuron development.

Here, we investigated *Pten* function during cortical interneuron development. Loss of *Pten* led to altered distribution of MGE-derived cells, neonatal interneuron death and an overall loss in interneurons. However, preferential loss of SST^+ interneurons led to an increased ratio of PV/SST in surviving interneurons in the adult mutant cortex, with ectopic PV^+ processes in layer I. Many of these phenotypes were cell autonomous. We also developed a method to virally modify MGE cells before transplantation to study the function of human ASD alleles, and found that *PTEN* ASD alleles were hypomorphic for multiple phenotypes.

Results

Pten loss in the MGE leads to increased AKT signaling

To determine its role in GABAergic cortical interneuron development, we generated *Pten* conditional knockouts (cKOs) from the medial ganglionic eminence (MGE) and preoptic area (POA) progenitors by crossing $Pten^{Flox}$ (Suzuki et al., 2001) to *Nkx2.1-Cre* (Xu et al., 2008) mice. The *Ai14* Cre-dependent reporter (Madisen et al., 2010) was used to follow cells that expressed Cre (tdTomato is expressed after Cre-mediated recombination). The *Nkx2.1-Cre* BAC transgenic drives expression, beginning ~embryonic day (E) 9.5, in most of the ventricular zone (VZ) of the MGE and POA (Figures S1A–S1C). At E12.5, Pten was globally expressed in the brains of WT and $Pten^{Flox/+}$ mice, including in the MGE (Figures S1D, S1E, S1G and S1H). Efficient loss of Pten protein occurred in early progenitors of the VZ and their progeny in the *Nkx2.1-Cre* lineage domains (Figures S1C, S1F and S1I).

Since loss of *Pten* leads to increased phosphorylated Akt (pAkt) and pGSK3beta in neurons (Kwon et al., 2006), we probed E13.5 MGE tissues for pAKT and pGSK3beta. Indeed, pAkt was increased ~3.5 fold at $serine^{473}$ ($p = 0.02$) and ~3 fold at $threonine^{308}$ ($p = 0.01$) (Figure S1J). Moreover, pGSK3beta at $serine^{9}$ was increased ~1.6-fold in *Pten* cKOs ($p = 0.03$) (Figure S1J). These data demonstrate a role for Pten signaling in regulating the Akt pathway in the embryonic MGE.

Pten loss in GABAergic cortical interneuron progenitors differentially effects SST and PV interneurons

Nkx2.1-Cre^{+}*; Pten* cKOs survive into adulthood but weighed ~25% less than their WT and *Pten*$^{Flox/+}$ littermates at P30 (Figure 1A). In contrast to other *Pten* mutants (Kwon et al., 2006), the brains of *Nkx2.1-Cre*$^{+}$*; Pten* cKOs were not altered in shape or size (Figure 1A). First, we counted the number of *Nkx2.1*-Cre-lineage cortical interneurons in the somatosensory cortex. At P30, there was ~53% reduction in the total number of *Nkx2.1-Cre*-lineage cells (Figures 1B–1G, 1H and Table S1). Next, we assessed the proportion of the two main subgroups of MGE-derived interneurons via expression of somatostatin (SST) and parvalbumin (PV) in the remaining tdTomato^{+} cells. The % tdTomato^{+} cells that were SST^{+} decreased 34% in *Pten* cKO neocortices (Figures 1B–1G and 1I, $p = 0.01$). Yet, the % tdTomato^{+} cells that were PV^{+} increased 39% (Figures 1E–1G, 1J, $p = 0.009$). This disproportionate effect on SST^{+} and PV^{+} interneuron numbers resulted in a greater PV to SST ratio in the P30 cortex (Figure 1K, $p = 0.01$), as well as in striatum and hippocampus (Table S1). Moreover, in *Pten* cKOs, the SST^{+} neuropil was greatly reduced in layer I, whereas the PV^{+} neuropil, which normally was restricted to neocortical layers II–VI, ectopically projected into layer I and displayed prominent PV^{+} puncta (Figures 1E′–1G′).

Nkx2-1-Cre removed *Pten* from the stem cells in the VZ. Next, we used *DlxI12b-Cre* (Potter et al., 2009) to remove *Pten* from secondary progenitors in the subventricular zone (SVZ) of the entire subpallium. At E15.5, Pten protein was detected in the VZ, but not the SVZ or neuronal layers of the basal ganglia (Figure S2A–S1A″ and S2B–S2B″). At P18, the % tdTomato^{+} cells that expressed VIP, a marker of CGE-derived interneurons, was unchanged (Figures S2C–S2E and S2L).

Similar to *Nkx2.1-Cre* cKOs, the % tdTomato^{+} cells in the *DlxI12b-Cre* cKOs that expressed SST decreased by 32% (Figures S2F–S2H and S2M, $p = 0.004$). Moreover, there was a trend for an increased % tdTomato^{+} cells that expressed PV (increased 24%, but did not reach statistical significance) (Figures S2I–S2K and S2N). Like the *Nkx2.1-Cre* cKOs, there was a trend for fewer total tdTomato^{+} cells in the neocortex (Figure S2O). Overall, *DlxI12b-Cre* cKOs had an increased PV^{+}/SST^{+} ratio of neocortical interneurons (Figure S2P, $p = 0.01$). These mutants also had ectopic PV^{+} projections in neocortical layer I at P18 (Figures S2I′–S2K′). Unfortunately, these mice could not be analyzed at later stages because they die soon after P18 for unknown reasons.

Pten loss in progenitors but not postmitotic interneurons decreased SST^{+} numbers

Pten loss, beginning in either the VZ (*Nkx2.1-Cre*) and/or SVZ (*DlxI12b-Cre*), led to a preferential loss of SST^{+} interneurons, while PV^{+} interneurons composed most of the remainder. To test if *Pten* was required in postmitotic SST^{+} cells, we used a *SST-IRES-Cre* mouse line (Taniguchi et al., 2011), which expresses Cre in MGE-derived SST^{+} cells as they leave the MGE (Figure 2A). Somatosensory cortices were assessed at P30 for *SST-IRES-Cre*-lineages (tdTomato^{+}). In contrast to *Nkx2.1-Cre* and *DlxI12b-Cre Pten* cKOs, *SST-IRES-Cre* cKOs did not show interneuron loss (Figure 2H), had no change in % tdTomato^{+} interneuronss that were SST^{+} or PV^{+} (Figures 2B–2I) and had no ectopic PV^{+} neuropil in layer I (Figures 2E–2G). These data demonstrate that the *Pten* phenotypes observed using

Nkx2.1-Cre and *DlxI12b-Cre* are caused by *Pten* loss in progenitor cells, which in turn led to changes in the PV/SST ratio.

Normal proliferation in *Pten* cKOs

The reduced numbers of interneurons in the neocortex of *Nkx2.1-Cre*$^{+}$*; Pten*$^{Flox/Flox}$ cKOs could be due to altered proliferation or apoptosis. We evaluated proliferation in the MGE by assessing phospho-histone-3 (PH3) expression and EdU incorporation, measures of M and S phase, respectively. The total number of PH3^{+} cells within the VZ and SVZ of the *Nkx2.1-Cre* domain of the MGE, (tdTomato^{+}), was counted at E11.5, E12.5 and E15.5; no changes in PH3^{+} cells were found (Figures S3A–S3I). Next, we administered a 30 minute pulse of EdU at E11.5, E12.5 and E15.5 and counted the density of EdU^{+} cells in the MGE's VZ and SVZ MGE. Lack of *Pten* had no effect (Figures S3J–S3R), suggesting normal proliferation.

Differential distribution and death of SST^{+} cells in *Pten* cKOs

To determine if *Pten* cKOs showed early changes in cell fate, we assessed the proportion of tdTomato^{+} cells that expressed SST at E12.5 and E15.5. At E12.5, there were no changes in the number or proportion of SST^{+} cells assayed using *in situ* hybridization or antibody staining (data not shown). However, by E15.5, the % of tdTomato^{+} cells that expressed SST was increased ~45% in the lateral cortex (Figures 3A–3I, $p = 0.02$), and decreased ~30% in the neocortex (Figures 3A, 3B, 3J–3P, $p = 0.006$ total, $p = 0.002$ MZ, $p = 0.02$ CP), suggesting that SST^{+} cKO interneurons were biased to occupy the lateral cortex.

Next, we assessed if *Pten* cKO cortical interneurons were susceptible to apoptosis, by testing for expression of cleaved caspase-3 (cC3). While we did not detect changes in apoptosis at E15.5, by E17.5 cC3^{+} cells were readily detected in ~13% of tdTomato^{+} marginal zone (MZ) *Pten* cKO cells, in both the neocortex and lateral cortex (controls had <1%; data not shown). By P0, ~36% of *Pten* cKO tdTomato^{+} cells in the MZ of the lateral cortex were cC3^{+} (Figures 3Q–3V and 3X, $p < 0.001$).

In the postnatal neocortex, there was progressive loss of MGE-derived (tdTomato^{+}) interneurons in the *Pten* cKOs: 10% at P0, 47% at P8 and 53% at P30 (Figure 1H). Thus, interneuron apoptosis primarily occurred between E17.5-P8. Interestingly, apoptosis was restricted to the cortical MZ, suggesting that interneuron death may occur due to an inability to integrate into the cortex.

Finally, we asked if SST^{+} or SST^{-} interneurons were differentially affected by apoptosis, by calculating the % of cC3^{+}/tdTomato^{+} cells in the MZ that were either SST^{+} or SST^{-}. Although SST^{-} cells were cC3+, cC3^{+}/tdTomato^{+} cells in the MZ of *Pten* cKOs were ~2-fold more likely to be SST^{+} (Figure 3X, $p < 0.001$ all conditions). This provided evidence that SST^{+} interneurons lacking *Pten* are more susceptible to apoptosis than SST^{-} interneurons. Moreover, at P0, the % tdTomato^{+} cells that expressed SST in the lateral cortex was reduced 26% (Figure 3W, $p = 0.02$), consistent with the evidence noted above that this was the period of interneuron death.

Since SST^{+} and PV^{+} neurons are the two primary MGE-derived cell types, the tdTomato^{+}/SST^{-} cells are likely to become PV^{+} cells. Although there is no early marker for

PV^+ interneurons, there is evidence that the majority of immature MGE cells that express SST will become SST^+. (Taniguchi et al., 2011; Vogt et al., 2015). Thus, prenatal expression of SST in the MGE-lineage is correlated with a SST^+ fate, and we propose that SST^+ embryonic *Pten* cKO cells are more susceptible to apoptosis than those that are SST^- (likely PV^+ fate).

Nkx2.1-Cre; Pten cKOs exhibit increased inhibition onto neocortical pyramidal neurons, deficits in social interaction and changes in EEG gamma oscillations

We next examined if *Pten* loss in interneurons altered the amount of inhibition received by neocortical excitatory neurons. Electrophysiological recordings were made of inhibitory inputs onto excitatory neurons in neocortical layers II/III at P30 (schema, Figure 4A). Despite the loss of half of the MGE-derived interneurons (Figure 1), there was ~2-fold increase in the frequency of spontaneous inhibitory post synaptic currents (IPSCs) onto layer II/III excitatory neurons in *Nkx2.1-Cre;* $Pten^{Flox/Flox}$ mice (Figure 4C, $p = 0.02$) but no change in amplitude between groups (Figure 4D). Example IPSCs recordings are shown for $Pten^{+/+}$ and $Pten^{Flox/Flox}$ (Figure 4B). These data demonstrate that spontaneous inhibitory tone is increased in layers II/III of *Pten* mutants.

Next, we performed a series of behavioral assays on *Nkx2.1-Cre; Pten* cKOs at P30. *Pten* cKOs were similar to WTs in the open field (Figures 5A–C), and the elevated plus maze (Figures 5D, 5E), suggesting normal levels of exploratory activity, locomotion and anxiety. However, *Pten* cKOs spent less time with novel mice in a social interaction test (Figure 5F, $p = 0.03$), and with a novel object (Figure 5I, $p = 0.05$). Interestingly, *Pten* cKOs had elevated EEG power during social interaction, with the greatest effect in the gamma frequency range (Figure 5G, $p = 0.005$). The baseline EEG was also recorded before the social interaction test and exhibited less power in the gamma frequency range in *Pten* cKOs (Figure 5H, $p = 0.04$). Overall, these data demonstrated that loss of *Pten* in cortical interneurons results in abnormal social behavior and altered EEG oscillations, within the gamma frequency band, both at baseline and during a task.

Cell autonomous role for *Pten* in regulating cortical interneuron soma size and interneuron subgroup ratios

To assess the cell autonomous role for *Pten* on cortical interneuron development, we utilized an MGE cell transplantation assay (Alvarez-Dolado et al., 2006). E12.5 *DlxI12b-*Cre^+*;* $Ai14^{Flox/+}$ MGE cells from $Pten^{+/+}$, $Pten^{Flox/+}$ or $Pten^{Flox/Flox}$ embryos were transplanted into WT P1 host neocortices and assessed at 35 days post transplant (DPT) (Figure 6A). Transplanted $Pten^{Flox/Flox}$ MGE cells had increased soma area (Figures 6B–6G) compared to both $Pten^{+/+}$ and $Pten^{Flox/+}$ (Figure 6H, $p < 0.0001$, both conditions).

Similar to the cKOs, transplanted *Pten* cKO MGE cells had a decreased proportion of SST^+ cells (Figures 6B–6D and 6I, $Pten^{Flox/+}$ $p = 0.002$, $Pten^{Flox/Flox}$ $p = 0.0001$), and increased PV^+ cells (Figures 6E–6G and 6J, $p = 0.02$). The transplanted MGE cells were also assayed for proteins that are expressed in specific MGE-derived interneuron groups: KV3.1, a channel predominantly expressed in PV^+ fast-spiking neurons (Du et al., 1996), as well as Reelin and Npas1 (which are expressed in a subpopulation of SST^+ but not PV^+,

interneurons) (Pesold et al., 1999; Stanco et al., 2014). The % transplanted *Pten*$^{Flox/Flox}$ MGE cells that expressed KV3.1 was increased (Figures S4A, S4D and S4G, $p = 0.001$). In conjunction, the % of cells expressing Reelin (Figures S4B, S4E and S4H, $p = 0.01$) and Npas1 (Figures S4C, S4F and S4I, $p = 0.006$) were decreased in *Pten*$^{Flox/Flox}$ MGE transplants, consistent with a reduction of SST^+ interneurons.

We next assessed the cell intrinsic physiological properties of the transplanted cells at 45 DPT (Table S3). Despite decreased AP threshold and resting membrane potential in transplanted *Pten* cKO MGE cells, the majority of cell intrinsic firing properties (i.e. FI slope, adaption ratio and action potential half-width) between WT and *Pten* cKOs were similar. Together, with the ectopic PV^+ processes in neocortical layer I and increased IPSC frequency onto excitatory neurons, these data suggest that *Pten* cKO cells primarily increased inhibitory tone via an overgrowth mechanism rather than by increased cell intrinsic excitability.

An *in vivo* complementation assay of *PTEN* ASD alleles demonstrates functional deficits in cortical interneuron development

Since the increased PV/SST ratio was a prominent phenotype in multiple brain regions (Table S1) and was cell autonomous (Figure 6), it was an ideal phenotype to test if human *PTEN* ASD alleles were functionally deficient. A major roadblock in ASD research is the lack of efficient screening assays for human alleles found in autism populations, particularly those with the power to test allele function *in vivo* during brain development. To circumvent this problem, we improved upon methods to introduce genes of interest into MGE cells before transplantation for *in vivo* development (Vogt et al., 2014) that combine Cre-dependent gene-deletion and activation of a fluorescent reporter in the transduced MGE cells (Vogt et al., 2015) with expression of an allele. In this manner, a WT or ASD allele is expressed while simultaneously deleting the corresponding endogenous gene. First, donor MGE cells that harbor a floxed gene of interest are transduced with a lentivirus, then transplanted into a WT host, allowing the modified cells to develop *in vivo*. This strategy challenges an ASD allele to complement the phenotypes of the gene deletion. Moreover, by using the *DlxI12b* enhancer that drives expression in the majority of GABAergic cortical neurons (Potter et al., 2009), we could study the effects of alleles only in GABAergic lineages. To this end, we generated lentiviruses with the *DlxI12b* enhancer (Arguello et al., 2013; Vogt et al., 2014), followed by a beta-globin minimal promoter driving *Cre* alone, with WT human *PTEN*, or with *PTEN* ASD alleles (Figure S5A). To test the fidelity of this assay, five previously reported *PTEN* alleles, identified in patients with *PTEN*-related syndromes and diagnosed with ASD (Butler et al., 2005; Orrico et al., 2009) were chosen for comparison to WT *PTEN*. Each vector was expressed in HEK293T cells and assayed for Akt activity, via phosphorylation at Ser^{473} (Figure S5B). Expression of WT *PTEN* efficiently decreased the level of pAkt. However, none of the *PTEN* ASD mutants were able to efficiently inactivate Akt, suggesting that they are less functional than WT *PTEN*.

To assess the function of the *PTEN* ASD alleles in cortical interneuron development, we transduced MGE cells with the aforementioned viruses before transplantation (schema, Figure 7A). E12.5 MGE cells that were either *Ai14*$^{Flox/+}$ (controls) or *Pten*$^{Flox/Flox}$;

Ai14$^{Flox/+}$, were transduced with *DlxI12b-Cre* lentiviruses (Figure S5A). These cells were then transplanted into P1 WT neocortices and developed *in vivo* until 35 days post transplant (DPT). *Cre* will result in the expression of tdTomato from the *Ai14* locus and will delete endogenous *Pten* from *Pten*$^{Flox/Flox}$ MGE cells. Since a *PTEN* allele is expressed from the same vector, the effect of either overexpression (via transduction of control MGE cells) or complementation (via transduction of *Pten*$^{Flox/Flox}$ MGE cells) can be assessed.

We first assessed if overexpressing WT or *PTEN* ASD alleles in control MGE cells changed the numbers of PV$^+$ neurons (Schema, Figure 7A). Interestingly, expression of WT *PTEN*, but not the *PTEN* ASD alleles, decreased the proportion of PV$^+$ cells (Figure 7B–7I, p = 0.002), suggesting that *PTEN* dosage influences this phenotype. Next, we assessed if *PTEN* ASD alleles could complement the increased % of transplanted cells that are PV$^+$ in *Pten* cKO MGE cells. Transduction of *Pten*$^{Flox/Flox}$ MGE cells led to an increased % of PV$^+$ cells compared to control cells with *Cre* only (Figures 7B, 7B′, 7I, 7J and Table S2), consistent with earlier data (Figures 1 and S2). Complementation with WT *PTEN* efficiently restored the % of PV$^+$ cells to control levels (Figures 7C′ and 7J, p = 0.0006). Notably, the *PTEN* ASD mutants were unable to complement the increased % of PV$^+$ cells and many were indistinguishable from *Cre* alone. Moreover, they differed from WT *PTEN* (Figures 7C′–7H′ and 7J, p = 0.002 *Pten*^{H118P}, p = 0.003 *Pten*^{Y176C}, p = 0.0001 *Pten*^{F241S}, p = 0.005 *Pten*^{D252G}). While WT and *PTEN* ASD mutants showed clear distinctions, there was no evidence of a dominant-negative effect induced by *PTEN* ASD mutants when expressed in control MGE cells. These data showed a role for *PTEN* dosage in regulating PV$^+$ interneuron ratios and that *PTEN* ASD alleles are deficient in complementing this phenotype.

The % of transplanted cells that were SST$^+$ were assessed in the same manner (Figures S6A–S6I). SST$^+$ cells were reduced ~15% in *Pten*$^{Flox/Flox}$ MGE cells compared to control cells transduced with *Cre* only (S6H–I and Table S2), and the % of *Pten*$^{Flox/Flox}$ cells that were SST$^+$ increased when complemented with WT *PTEN* (Figure S6I, p = 0.02). However, some of the *PTEN* ASD alleles did not complement the decreased % of SST$^+$ cells (Figure S6I, p = 0.02 *PTEN*^{Y176C}, p = 0.009 *PTEN*^{D252G}).

Loss of *Pten* function increases cell size, including the cell bodies (somas) of neurons (Kwon et al., 2006; and Figure 6H). Thus, we compared the function of WT and *PTEN* ASD alleles with regards to soma area. As expected, deletion of *Pten* by transduction with *Cre* led to increased soma areas in *Pten*$^{Flox/Flox}$ MGE cells (Figure S6K). Next, we quantified soma area after transduction with *PTEN* ASD alleles; each were less efficient than WT *PTEN* at preventing the increase in soma area of *Pten*$^{Flox/Flox}$ MGE cells (Figure S6K, $p < 0.0001$ for WT *PTEN*, *PTEN*^{H118P} and *PTEN*^{Y176C}, p = 0.04 for *PTEN*^{F241S} and p = 0.0005 for *PTEN*^{D252G}). Finally, we transduced *PTEN* or the ASD alleles into WT MGE cells, and found no change in soma area with any allele (Figure S6J). Consistent with earlier data (Figure 7I and S6H), these results suggest that the *PTEN* ASD alleles do not act in a dominant fashion. Together, these data revealed a role for human *PTEN* ASD alleles in regulating cortical interneuron ratios, cell size, and demonstrated a functional *in vivo* assay to test the impact each mutant imparts to development.

Discussion

Pten is required to obtain normal numbers of SST^+ and PV^+ cortical interneurons, the two main subgroups of MGE-derived interneurons. Loss of *Pten* led to apoptosis that preferentially affected neonatal SST^+ interneurons. This resulted in an increased PV^+/SST^+ ratio, as well as ectopic PV^+ projections and a paucity of SST^+ axons in cortical layer I. *Pten* mutants also had a decreased E/I ratio in neocortical layers II/III, and reduced social behaviors. Finally, an MGE transplantation/complementation assay showed that *PTEN* ASD alleles were hypomorphic *in vivo*.

Pten regulates the number and ratio of SST and PV interneurons

Pten deletion in MGE progenitors of the VZ (via *Nkx2.1-Cre*) resulted in a greater reduction in SST^+ compared to PV^+ interneurons in the neocortex (Table S1). While this phenotype was also seen when *Pten* was deleted in the SVZ (via *DlxI12b-Cre*, Figure S2), no interneuron loss was observed using *SST-IRES-Cre* (Figure 2), which begins to express as these cells become postmitotic, suggesting that *Pten* regulation of interneuron numbers depends on its function in progenitors. The increased PV/SST ratio was also observed in MGE transplantation assays (Figures 6, 7, S6) consistent with a cell autonomous role for *Pten*.

The altered PV/SST ratio is likely due to preferential cell death of SST^+ cells during late gestation and neonatal ages, rather than a change in cell fate or proliferation. In support of this, we did not observe changes in the proportion of SST^+ MGE-derived cells at early embryonic ages (E12.5) or in proliferation (Figure S3). At E15.5, more SST^+ interneurons occupied the lateral cortex and were depleted from the neocortex (Figure 3). By P0, there was elevated apoptosis that preferentially affected SST^+ neurons in both the lateral and neocortex marginal zones, a time just before the major loss in interneurons were decreased in the neocortex (Figure 1H).

Alterations (increases and decreases) in cortical interneurons have been reported in ASD mouse mutants (Durand et al., 2012; Karayannis et al., 2014; Peñagarikano et al., 2011; Selby et al., 2007; Gogolla et al., 2014, Allegra et al., 2014). Thus, defects in interneuron numbers may be found in some forms of ASD, and the PV/SST ratio should be measured in ASD patients. Moreover, further work should be done in mice to elucidate the mechanisms that control the numbers of PV and SST interneurons. Some insights have been garnered from the analysis of mouse transcription factor mutants that exhibit altered PV/SST ratios, including *Dlx1* (Cobos et al., 2005), *Lhx6 (*Neves et al., 2013), *Npas1&3* (Stanco et al., 2014), *Olig1* (Silbereis et al., 2014) and *Satb1* (Close et al., 2012; Denaxa et al., 2012). While the role of these TFs in neuropsychiatric disorders are obscure, alleles of some of these genes have been associated with disorders (Hamilton et al., 2005, Stanco et al., 2014).

Pten regulates the morphology and connectivity of SST and PV interneurons

Interestingly, PV^+ processes ectopically grew into neocortical layer I, suggesting that *Pten* restrains the spatial distribution and perhaps connectivity of PV^+ axons. Loss of *Pten* in excitatory neurons likewise results in overgrowth of their processes (Kwon et al., 2006).

Given that layer I contains the apical dendrites of pyramidal neurons, the excessive PV^+ processes could impact the nature and number of inhibitory inputs onto excitatory neurons. Indeed, loss of *Pten* in MGE-derived GABAergic cortical interneurons resulted in elevated spontaneous inhibitory tone on cortical layer II/III pyramidal neurons (Figure 4), despite the ~50% reduction in MGE-derived interneurons (Figure 1, Table S1). We hypothesize that the overgrowth of PV^+ processes in layer I may underlie the increased inhibition. Interestingly, increased inhibitory tone has been observed in other mouse mutants of ASD genes that repress the PI3K/Akt/mTor pathway, including *NF1* (Costa et al., 2002; Cui et al., 2008), suggesting that reducing the E/I ratio, through increased inhibition, may be an important mechanism underlying the effects of some ASD genes. Other ASD mouse models have increased E/I (Gogolla et al., 2014); thus various mechanisms that disrupt E/I away from the optimal range, in either direction, may account for cortical dysfunction.

PV^+ interneurons are necessary and sufficient for gamma oscillations (Cardin et al., 2009; Sohal et al., 2009), and various (depressed and elevated) alterations have been observed in individuals with ASD (Gandal et al., 2010; Orekhova et al., 2007; Wilson et al., 2007). In *Pten* cKO mice, we observed reduced gamma rhythms at rest and increased when performing a task (Figure 5). Finally, *Pten* mutants had deficits in social interaction (Figure 5), supporting the hypothesis that some behavioral and cognitive phenotypes may be caused by E/I imbalance (Rubenstein and Merzenich, 2003).

Loss of *Pten* in excitatory neurons led to phenotypes that were distinct from those observed from deletion in GABAergic cortical interneurons, including macrocephaly, increased excitation and seizures (Kwon et al., 2006). Moreover, *Pten* deletion in either neuron type resulted in hyperactivated Akt and hypertrophy, suggesting that while different global phenotypes may be attributed to certain cell types, some cellular phenotypes were common between inhibitory and excitatory neurons (hyperactivated Akt, soma and neurite hypertrophy).

An *in vivo* complementation assay to screen functional changes in ASD alleles

Due to the many risk alleles found in ASD (Murdoch and State, 2013; Tebbenkamp et al., 2014), we developed an efficient means to screen ASD alleles for functional deficits *in vivo.* This was performed in cortical interneurons, a cell type implicated in ASD and other neuropsychiatric disorders. A standard way to study an ASD allele is to create a knock-in mouse, which is low-throughput process. Our complementation assay tests cell autonomous effects of ASD alleles in ~two months, and can rapidly investigate molecular, developmental, morphological and electrophysiological parameters *in vivo*. While this assay requires mouse null mutants, it is now relatively easy to obtain these animals. In addition, the modular design of the lentiviral vector (Figure S5) permits the use of any enhancer or promoter, which could facilitate assaying functions specific to cell-type. Moreover, any gene can be inserted downstream of the *Cre* cassette. We suggest that this assay will be of great utility for *in vivo* functional characterization of any mutant allele.

Our assay showed that all five of the tested human *PTEN* ASD alleles were hypomorphic, based upon their reduced activity to rescue two phenotypes: increased soma area and PV/SST ratio (Figures 7 and S6). Consistent with our results, an assay of these alleles in

yeast provided evidence that they had reduced phosphatase function but not as low as *PTEN* alleles discovered in various cancers (Rodríguez-Escudero et al., 2011). Furthermore, these alleles did not have dominant functions when assayed in WT interneurons (Figures 7 and S6). In sum, our experiments delineate a major role for *PTEN* in the survival, connectivity and PV/SST ratio of GABAergic cortical interneurons. These findings provide insights into how deficits in *PTEN* contribute to ASD, and suggests that PI3K/Akt/mTor signaling differentially regulates PV and SST interneuron development.

Experimental procedures

Animals

All mice have been described: *Ai14* Cre-reporter (Madisen et al., 2010), *Nkx2.1-Cre* (Xu et al., 2008), *SST-IRES-Cre* (Taniguchi et al., 2011), *DlxI12b-Cre* (Potter et al., 2009), $Pten^{flox}$ (Suzuki et al., 2001). Mice were initially on a mixed C57BL6/J, CD-1 background. All lines, except *SST-IRES-Cre*, were backcrossed to CD-1 for at least four generations before analysis. *SST-IRES-Cre* males were maintained on a C57Bl6/J background. For timed pregnancies, noon on the day of the vaginal plug was counted as embryonic day 0.5. All animal care and procedures were performed according to the University of California at San Francisco Laboratory Animal Research Center guidelines.

Behavior

Open-field test—An individual mouse was placed near the wall-side of 50 × 50 cm open-field arena, and the movement of the mouse was recorded by a video camera for 10 min. The recorded video file was later analyzed with Any-Maze software (San Diego Instruments). Time in the center of the field (a 25 × 25 cm square), and distances travelled in the center and perimeter were measured. The open field arena was cleaned with 70% ethanol and wiped with paper towels between each trial. Investigators were blind to genotype during scoring of videos.

Elevated plus maze test—A mouse was placed at the junction of the open and closed arms, facing the arm opposite to the experimenter, of an apparatus with two open arms without walls (30 × 5 × 0.5 cm) across from each other and perpendicular to two closed arms with walls (30 × 5 × 15 cm) with a center platform (5 × 5 cm), and at a height of 40 cm above the floor. Mouse movement was recorded by video for 10 min and analyzed for the first 5 min. The video file was analyzed, and time and number of entries in the open arms of the apparatus was measured. The elevated plus maze apparatus arms were cleaned with 70% ethanol and wiped with paper towels between each trial. Investigators were blind to genotype during scoring of videos.

Social interaction task—Mice were connected to the EEG preamplifier, and then habituated in their homecage for 15 min before beginning the task. After habituation, we recorded baseline EEG activity for 5 min. Then we introduced an age-matched mouse (3–4 weeks old, same gender) into the homecage of the subject mouse and allowed the freely-moving mice to interact for 5 minutes while continuing to record EEG activity. We recorded EEG using a time-locked video EEG monitoring system (Pinnacle Technology), enabling us

to subsequently correlate periods of social interaction (defined as sniffing, close following, and allo-grooming) with specific timepoints in the EEG recording. Investigators were blind to genotype during scoring of videos.

Novel object task—Following the social interaction task, the subject mouse was presented with a novel object (50 mL Falcon tube cap) for 5 minutes and the amount of time spent investigating the object was analyzed. Investigators were blind to genotype during scoring of videos.

Data analysis for EEGs were performed in Matlab (The MathWorks) using custom written software. To analyze changes in power during the baseline period (which occurred just before the social interaction task), a 2-way ANOVA was used and found to be significant for genotype if ($p<0.001$), frequency if ($p<0.001$), and genotype × frequency if ($p<0.05$). Differences between genotypes for each frequency band was tested using Student's two-tailed, unpaired *t*-tests. To analyze differences in social interaction-evoked power, we used repeated measures ANOVA with mouse, task condition (baseline vs. social interaction), and genotype × condition (baseline vs. social interaction) as factors.

Electrophysiology

Slice preparation—Slice preparation and intracellular recordings were performed as previously described (Sohal and Huguenard, 2005). Detailed methods can be found in extended experimental procedures.

Lentiviral production: Lentiviral production was performed as previously described (Vogt et al., 2014, Vogt et al., 2015). Detailed methods can be found in extended experimental procedures.

MGE transplantation: MGE transplantations were done as previously described (Vogt et al., 2014, Vogt et al., 2015). A detailed description can be found in extended experimental procedures.

Supplementary Material

Refer to Web version on PubMed Central for supplementary material.

Acknowledgments

This work was supported by grants to JLRR from: Autism Speaks, Nina Ireland, Weston Havens Foundation, NIMH R01 MH081880, and NIMH R37 MH049428. VSS was supported by the Staglin Family and International Mental Health Research Organization, NIH DP2 MH100011 and NIMH R01 MH100292. KKAC was supported by a NARSAD Young Investigator Award from the Brain and Behavior Foundation. ATL was supported by a Medical Scientist Training Program grant from NIGMS (GM07618).

References

Allegra M, Genovesi S, Maggia M, Cenni MC, Zunino G, Sgadò P, Caleo M, Bozzi Y. Altered GABAergic markers, increased binocularity and reduced plasticity in the visual cortex of Engrailed-2 knockout mice. Front Cell Neurosci. 2014; 17:163. [PubMed: 24987331]

Alvarez-Dolado M, Calcagnotto ME, Karkar KM, Southwell DG, Jones-Davis DM, Estrada RC, Rubenstein JLR, Alvarez-Buylla A, Baraban SC. Cortical inhibition modified by embryonic neural precursors grafted into the postnatal brain. J Neurosci. 2006; 26:7380–7389. [PubMed: 16837585]

Anderson SA, Eisenstat DD, Shi L, Rubenstein JL. Interneuron migration from basal forebrain to neocortex: dependence on Dlx genes. Science. 1997; 278:474–476. [PubMed: 9334308]

Arguello A, Yang XY, Vogt D, Stanco A, Rubenstein JLR, Cheyette BNR. Dapper Antagonist of Catenin-1 Cooperates with Dishevelled-1 during Postsynaptic Development in Mouse Forebrain GABAergic Interneurons. PLoS ONE. 2013; 8

Bourgeron T. A synaptic trek to autism. Curr Opin Neurobiol. 2009; 19:231–234. [PubMed: 19545994]

Butler MG, Dasouki MJ, Zhou X-P, Talebizadeh Z, Brown M, Takahashi TN, Miles JH, Wang CH, Stratton R, Pilarski R, et al. Subset of individuals with autism spectrum disorders and extreme macrocephaly associated with germline PTEN tumour suppressor gene mutations. J Med Genet. 2005; 42:318–321. [PubMed: 15805158]

Cardin JA, Carlén M, Meletis K, Knoblich U, Zhang F, Deisseroth K, Tsai LH, Moore CI. Driving fast-spiking cells induces gamma rhythm and controls sensory responses. Nature. 2009; 459:663–667. [PubMed: 19396156]

Chao HT, Chen H, Samaco RC, Xue M, Chahrour M, Yoo J, Neul JL, Gong S, Lu HC, Heintz N, et al. Dysfunction in GABA signalling mediates autism-like stereotypies and Rett syndrome phenotypes. Nature. 2010; 468:263–269. [PubMed: 21068835]

Close J, Xu H, De Marco Garcia N, Batista-Brito R, Rossignol E, Rudy B, Fishell G. Satb1 is an activity-modulated transcription factor required for the terminal differentiation and connectivity of medial ganglionic eminence-derived cortical interneurons. J Neurosci. 2012; 32:17690–705. [PubMed: 23223290]

Cobos I, Calcagnotto ME, Vilaythong AJ, Thwin MT, Noebels JL, Baraban SC, Rubenstein JL. Mice lacking Dlx1 show subtype-specific loss of interneurons, reduced inhibition and epilepsy. Nat Neurosci. 2005; 8:1059–68. [PubMed: 16007083]

Costa RM, Federov NB, Kogan JH, Murphy GG, Stern J, Ohno M, Kucherlapati R, Jacks T, Silva AJ. Mechanism for the learning deficits in a mouse model of neurofibromatosis type 1. Nature. 2002; 415:526–530. [PubMed: 11793011]

Cui Y, Costa RM, Murphy GG, Elgersma Y, Zhu Y, Gutmann DH, Parada LF, Mody I, Silva AJ. Neurofibromin Regulation of ERK Signaling Modulates GABA Release and Learning. Cell. 2008; 135:549–560. [PubMed: 18984165]

Denaxa M, Kalaitzidou M, Garefalaki A, Achimastou A, Lasrado R, Maes T, Pachnis V. Maturation-promoting activity of SATB1 in MGE-derived cortical interneurons. Cell Rep. 2012; 2:1351–62. [PubMed: 23142661]

Durand S, Patrizi A, Quast KB, Hachigian L, Pavlyuk R, Saxena A, Carninci P, Hensch TK, Fagiolini M. NMDA Receptor Regulation Prevents Regression of Visual Cortical Function in the Absence of Mecp2. Neuron. 2012; 76:1078–1090. [PubMed: 23259945]

Fraser MM, Bayazitov IT, Zakharenko SS, Baker SJ. Phosphatase and tensin homolog, deleted on chromosome 10 deficiency in brain causes defects in synaptic structure, transmission and plasticity, and myelination abnormalities. Neuroscience. 2008; 151:476–488. [PubMed: 18082964]

Gandal MJ, Edgar JC, Ehrlichman RS, Mehta M, Roberts TPL, Siegel SJ. Validating γ oscillations and delayed auditory responses as translational biomarkers of autism. Biol Psychiat. 2010; 68:1100–1106. [PubMed: 21130222]

Gogolla N, Takesian AE, Feng G, Fagiolini M, Hensch TK. Sensory Integration in Mouse Insular Cortex Reflects GABA Circuit Maturation. Neuron. 2014; 83:894–905. [PubMed: 25088363]

Hamilton SP, Woo JM, Carlson EJ, Ghanem N, Ekker M, Rubenstein JL. Analysis of four DLX homeobox genes in autistic probands. BMC Genet. 2005; 6:52. [PubMed: 16266434]

Han S, Tai C, Westenbroek RE, Yu FH, Cheah CS, Potter GB, Rubenstein JL, Scheuer T, De la Iglesia HO, Catterall WA. Autistic-like behaviour in Scn1a+/− mice and rescue by enhanced GABA-mediated neurotransmission. Nature. 2012; 489:385–390. [PubMed: 22914087]

Huang ZJ, Di Cristo G, Ango F. Development of GABA innervation in the cerebral and cerebellar cortices. Nat Rev Neurosci. 2007; 8:673–686. [PubMed: 17704810]

Karayannis T, Au E, Patel JC, Kruglikov I, Markx S, Delorme R, Héron D, Salomon D, Glessner J, Restituito S, et al. Cntnap4 differentially contributes to GABAergic and dopaminergic synaptic transmission. Nature. 2014; 511:236–40. [PubMed: 24870235]

Kölsch V, Charest PG, Firtel RA. The regulation of cell motility and chemotaxis by phospholipid signaling. J Cell Sci. 2008; 121:551–559. [PubMed: 18287584]

Kwon CH, Luikart BW, Powell CM, Zhou J, Matheny SA, Zhang W, Li Y, Baker SJ, Parada LF. Pten Regulates Neuronal Arborization and Social Interaction in Mice. Neuron. 2006; 50:377–388. [PubMed: 16675393]

Ljungberg MC, Sunnen CN, Lugo JN, Anderson AE, D'Arcangelo G. Dis. Model Mech. 2009; 2:389–98.

Luikart BW, Schnell E, Washburn EK, Bensen AL, Tovar KR, Westbrook GL. Pten knockdown in vivo increases excitatory drive onto dentate granule cells. J Neurosci. 2011; 31:4345–4354. [PubMed: 21411674]

Madisen L, Zwingman TA, Sunkin SM, Oh SW, Zariwala HA, Gu H, Ng LL, Palmiter RD, Hawrylycz MJ, Jones AR, et al. A robust and high-throughput Cre reporting and characterization system for the whole mouse brain. Nat Neurosci. 2010; 13:133–140. [PubMed: 20023653]

Marui T, Hashimoto O, Nanba E, Kato C, Tochigi M, Umekage T, Ishijima M, Kohda K, Kato N, Sasaki T. Association between the neurofibromatosis-1 (NF1) locus and autism in the Japanese population. Am J Med Genet B. 2004; 131:43–47.

Mbarek O, Marouillat S, Martineau J, Barthélémy C, Müh JP, Andres C. Association study of the NF1 gene and autistic disorder. Am J Genet B. 1999; 88:729–732.

Miyoshi G, Hjerling-Leffler J, Karayannis T, Sousa VH, Butt SJB, Battiste J, Johnson JE, Machold RP, Fishell G. Genetic fate mapping reveals that the caudal ganglionic eminence produces a large and diverse population of superficial cortical interneurons. J Neurosci. 2010; 30:1582–1594. [PubMed: 20130169]

Murdoch JD, State MW. Recent developments in the genetics of autism spectrum disorders. Curr Opin Genet Dev. 2013; 23:310–315. [PubMed: 23537858]

Neves G, Shah MM, Liodis P, Achimastou A, Denaxa M, Roalfe G, Sesay A, Walker MC, Pachnis V. The LIM homeodomain protein Lhx6 regulates maturation of interneurons and network excitability in the mammalian cortex. Cereb Cortex. 2013; 23:1811–23. [PubMed: 22710612]

O'Roak BJ, Vives L, Fu W, Egertson JD, Stanaway IB, Phelps IG, Carvill G, Kumar A, Lee C, Ankenman K, et al. Multiplex targeted sequencing identifies recurrently mutated genes in autism spectrum disorders. Science. 2012; 338:1619–1622. [PubMed: 23160955]

Orekhova EV, Stroganova TA, Nygren G, Tsetlin MM, Posikera IN, Gillberg C, Elam M. Excess of High Frequency Electroencephalogram Oscillations in Boys with Autism. Biol Psychiat. 2007; 62:1022–1029. [PubMed: 17543897]

Orrico A, Galli L, Buoni S, Orsi A, Vonella G, Sorrentino V. Novel PTEN mutations in neurodevelopmental disorders and macrocephaly. Clin Genet. 2009; 75:195–198. [PubMed: 18759867]

Peñagarikano O, Abrahams BS, Herman EI, Winden KD, Gdalyahu A, Dong H, Sonnenblick LI, Gruver R, Almajano J, Bragin A, et al. Absence of CNTNAP2 leads to epilepsy, neuronal migration abnormalities, and core autism-related deficits. Cell. 2011; 147:235–246. [PubMed: 21962519]

Potter GB, Petryniak MA, Shevchenko E, McKinsey GL, Ekker M, Rubenstein JLR. Generation of Cre-transgenic mice using Dlx1/Dlx2 enhancers and their characterization in GABAergic interneurons. Mol Cell Neurosci. 2009; 40:167–186. [PubMed: 19026749]

Rodríguez-Escudero I, Oliver MD, Andrés-Pons A, Molina M, Cid VJ, Pulido R. A comprehensive functional analysis of PTEN mutations: Implications in tumor- and autism-related syndromes. Hum Mol Genet. 2011; 20:4132–4142. [PubMed: 21828076]

Rubenstein JLR, Merzenich MM. Model of autism: increased ratio of excitation/inhibition in key neural systems. Genes Brain Behav. 2003; 2:255–267. [PubMed: 14606691]

Selby L, Zhang C, Sun QQ. Major defects in neocortical GABAergic inhibitory circuits in mice lacking the fragile X mental retardation protein. Neurosci Lett. 2007; 412:227–232. [PubMed: 17197085]

Silbereis JC, Nobuta H, Tsai HH, Heine VM, McKinsey GL, Meijer DH, Howard MA, Petryniak MA, Potter GB, Alberta JA, et al. Neuron. 2014; 81:574–87. [PubMed: 24507192]

Sohal VS, Huguenard JR. Inhibitory coupling specifically generates emergent gamma oscillations in diverse cell types. PNAS. 2005; 102:18638–43. [PubMed: 16339306]

Sohal VS, Zhang F, Yizhar O, Deisseroth K. Parvalbumin neurons and gamma rhythms enhance cortical circuit performance. Nature. 2009; 459:698–702. [PubMed: 19396159]

Stanco A, Pla R, Vogt D, Chen Y, Mandal S, Walker J, Hunt RF, Lindtner S, Erdman CA, Pieper AA, et al. NPAS1 Represses the generation of specific subtypes of cortical interneurons. Neuron. 2014; 84:940–53. [PubMed: 25467980]

Stiles BL. Phosphatase and tensin homologue deleted on chromosome 10: Extending its PTENtacles. Int J Biochem Cell B. 2009; 41:757–761.

Suzuki A, Yamaguchi MT, Ohteki T, Sasaki T, Kaisho T, Kimura Y, Yoshida R, Wakeham A, Higuchi T, Fukumoto M, et al. T cell-specific loss of Pten leads to defects in central and peripheral tolerance. Immunity. 2001; 14:523–534. [PubMed: 11371355]

Taniguchi H, He M, Wu P, Kim S, Paik R, Sugino K, Kvitsani D, Fu Y, Lu J, Lin Y, et al. A Resource of Cre Driver Lines for Genetic Targeting of GABAergic Neurons in Cerebral Cortex. Neuron. 2011; 71:995–1013. [PubMed: 21943598]

Tebbenkamp ATN, Willseya J, State MW, Sestan N. The developmental transcriptome of the human brain: implications for neurodevelopmental disorders. Curr Opin Neurol. 2014; 27:149–156. [PubMed: 24565942]

Vogt D, Hunt RF, Mandal S, Sandberg M, Silberberg SN, Nagasawa T, Yang Z, Baraban SC, Rubenstein JLR. Lhx6 Directly Regulates Arx and CXCR7 to Determine Cortical Interneuron Fate and Laminar Position. Neuron. 2014; 82:350–364. [PubMed: 24742460]

Vogt D, Wu P-R, Sorrells SF, Arnold C, Alvarez-Buylla A, Rubenstein JLR. Viral-mediated labeling and transplantation of medial ganglionic eminence (MGE) cells for in vivo studies. J Vis Exp. 2015:e52740.10.3791/52740

Williams MR, DeSpenza T Jr, Li M, Gulledge AT, Luikart BW. Hyperactivity of newborn Pten knock-out neurons results from increased excitatory synaptic drive. J Neurosci. 2015; 35:943–59. [PubMed: 25609613]

Wilson TW, Rojas DC, Reite ML, Teale PD, Rogers SJ. Children and Adolescents with Autism Exhibit Reduced MEG Steady-State Gamma Responses. Biol Psychiat. 2007; 62:192–197. [PubMed: 16950225]

Wiznitzer M. Autism and tuberous sclerosis. J Child Neurol. 2004; 19:675–9. [PubMed: 15563013]

Wonders CP, Anderson SA. The origin and specification of cortical interneurons. Nat Rev Neurosci. 2006; 7:687–696. [PubMed: 16883309]

Xu Q, Tam M, Anderson SA. Fate mapping Nkx2.1-lineage cells in the mouse telencephalon. J Comp Neurol. 2008; 506:16–29. [PubMed: 17990269]

Zhou J, Blundell J, Ogawa S, Kwon C-H, Zhang W, Sinton C, Powell CM, Parada LF. Pharmacological inhibition of mTORC1 suppresses anatomical, cellular, and behavioral abnormalities in neural-specific Pten knock-out mice. J Neurosci. 2009; 29:1773–1783. [PubMed: 19211884]

Highlights

- *Pten* regulates the ratio of PV^+/SST^+ cortical interneurons
- Loss of *Pten* increases PV^+ process growth and inhibition
- *Pten* interneuron cKOs have altered social behavior and gamma oscillations
- An *in vivo* screening assay tests human ASD allele function

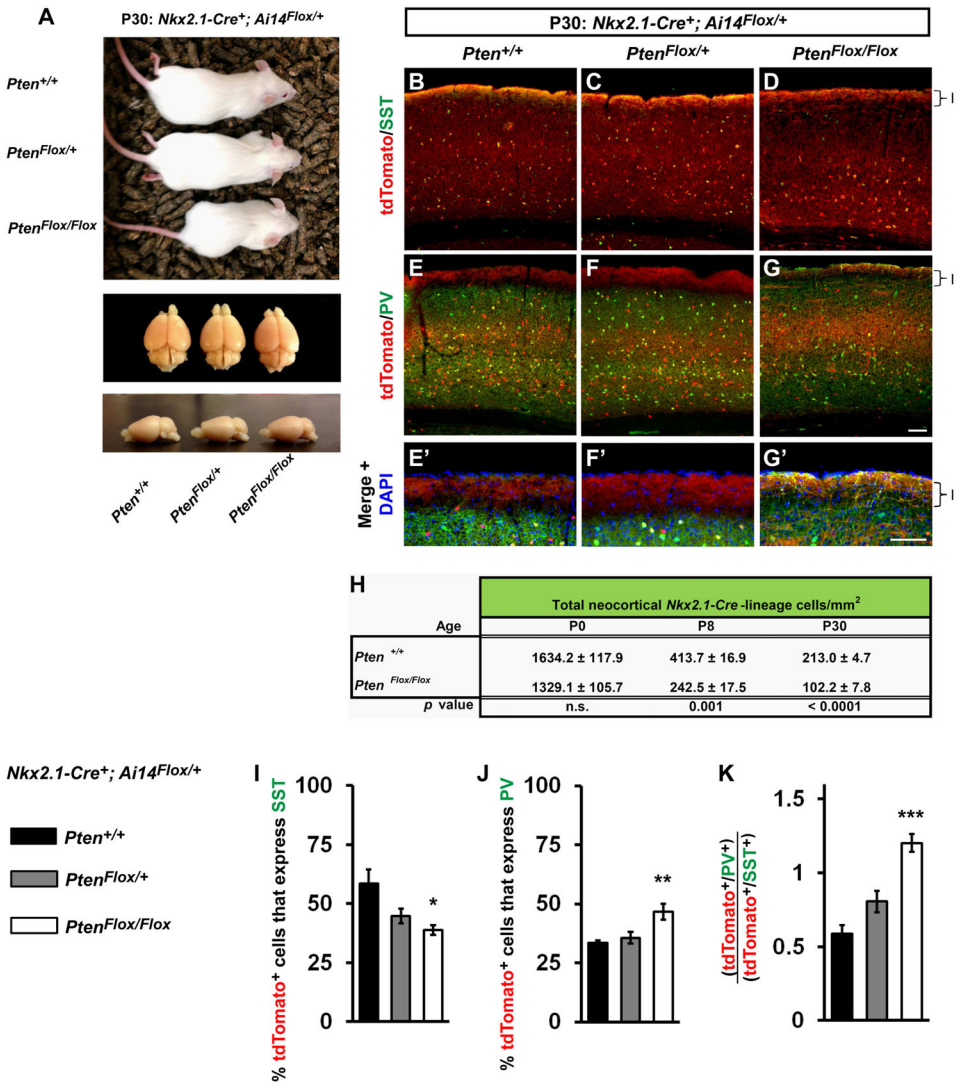

Figure 1. ***Nkx2.1-Cre; Pten*** **conditional mutants exhibit reduced interneuron numbers, increased PV/SST ratio and ectopic PV$^+$ processes in layer I**

(A) Images of postnatal day (P) 30 mice and brains (superior and lateral views) from *Pten*$^{+/+}$, *Pten*$^{Flox/+}$ and *Pten*$^{Flox/Flox}$ (*Nkx2.1-Cre*$^+$*; Ai14Flox/*$^+$) genotypes. Coronal immunofluorescent images of P30 somatosensory cortices show co-expression of tdTomato with SST (B–D) or with PV (E–G). (E′-G′) Higher magnification images of neocortical layer I from images E–G that have been merged with DAPI. Brackets to the right of each panel denote the boundaries of layer I. (H) Quantification of the number of tdTomato$^+$ cells per square millimeter (mm^2) in the somatosensory cortex over time. Quantification of the % tdTomato$^+$ cells that express either SST (I) or PV (J). (K) Ratio of tdTomato$^+$/PV$^+$ cells per mm^2 over tdTomato$^+$/SST$^+$ cells per mm^2 in the neocortex. Data are represented as mean ± SEM. *$p < 0.05$, **$p < 0.01$. Scale bars in (G and G′) = 100 μm. **See also** Figures S1, and S2, and Tables S1 and S2.

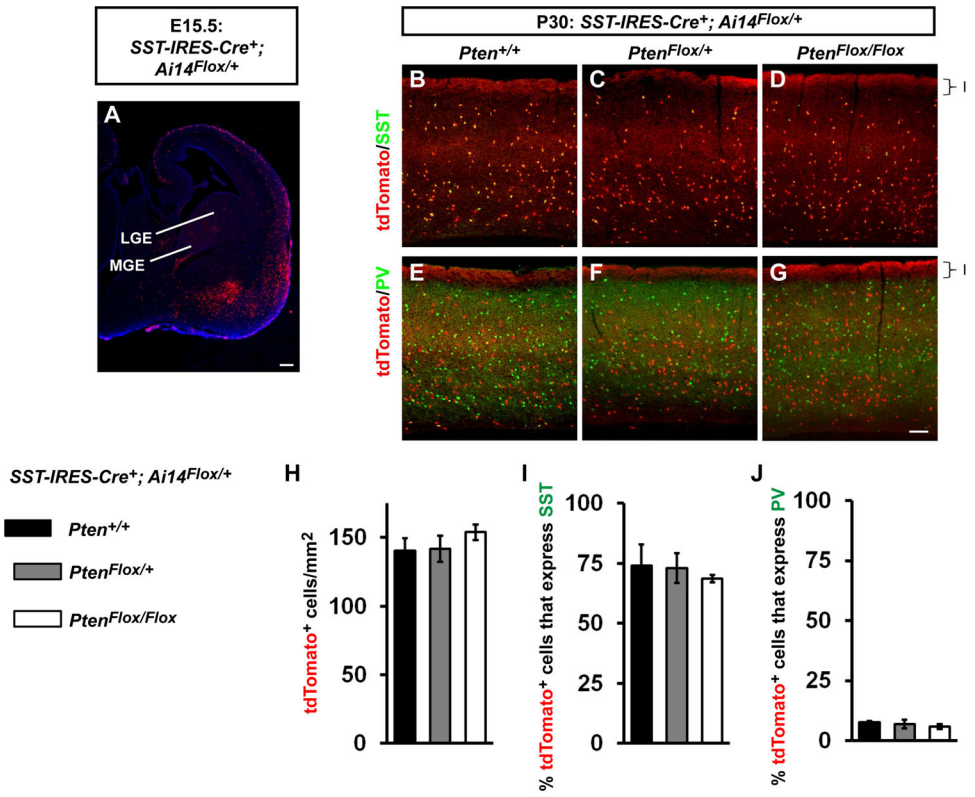

Figure 2. Normal interneuron numbers and morphology in *SST-IRES-Cre; Pten* cKOs

(A) Coronal immunofluorescent image of *SST-IRES-Cre*$^{+}$*; Ai14Flox/*$^{+}$ showing the pattern of SST-lineage cells (tdtomato^{+}) at embryonic day (E) 15.5. Coronal immunofluorescent images of P30 somatosensory cortices from *SST-IRES-Cre*$^{+}$*; Ai14Flox/*$^{+}$;*Pten*$^{+/+}$, *Pten*$^{Flox/+}$ and *Pten*$^{Flox/Flox}$ show expression of tdTomato with SST (B–D) or with PV (E–G). Brackets to the right of each panel denote the boundaries of layer I. (H) Quantification of the total number of tdTomato^{+} cells per mm^{2}. Quantification of the % tdTomato^{+} cells that express SST (I) or PV (J). Data are represented as mean ± SEM. Scale bars in (A and G) = 100 μm. **See also** Figure S2.

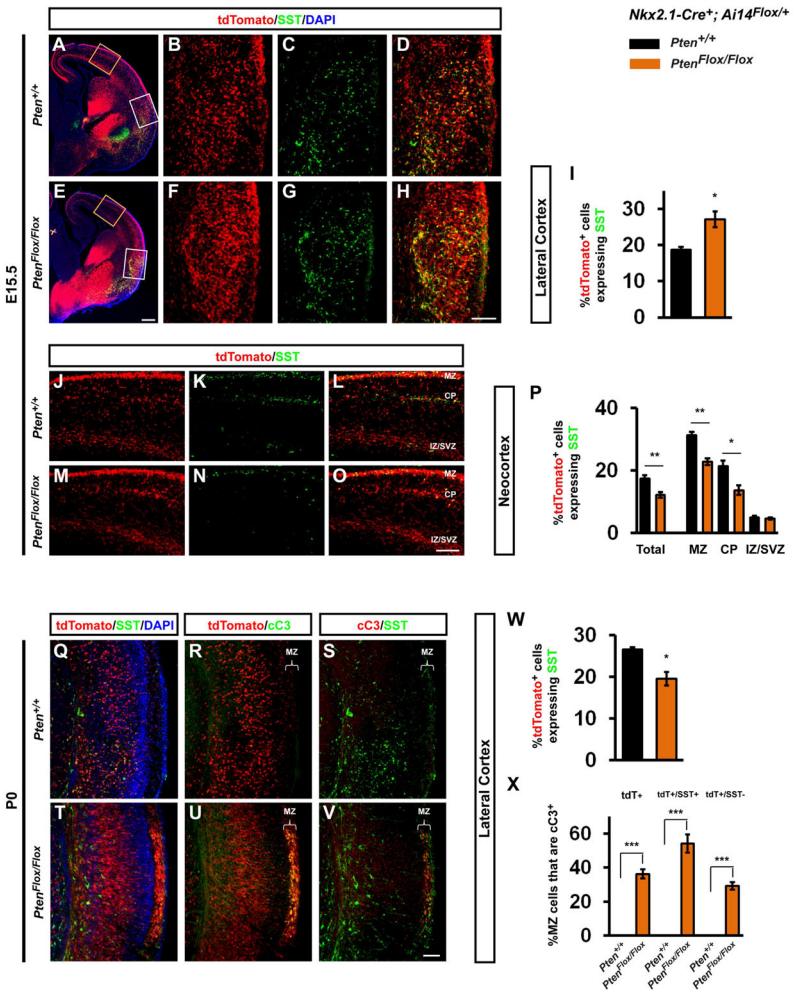

Figure 3. Abnormal distribution of SST$^+$ cells and elevated apoptosis in *Nkx2.1-Cre; Pten* cKOs

E15.5 coronal immunofluorescent images of *Nkx2.1-Cre*-lineage cells (tdTomato$^+$) colabeled for SST and DAPI in *Pten*$^{+/+}$ (A) and *Pten*$^{Flox/Flox}$ (E) brains. (B–D and F–H) Higher magnification fluorescent images of the lateral cortex (white boxes in A, E). (I) Quantification of the % tdTomato$^+$ cells that express SST in the lateral cortex. (J–O) Immunofluorescent images of the neocortex (orange boxes in A, E) showing tdTomato$^+$ cells that express SST. (P) Quantification of the % tdTomato$^+$ cells that express SST in the neocortex. (Q–V) Immunofluorescent images of the lateral cortex at P0 showing tdTomato$^+$ cells that express SST and cleaved-caspase-3 (cC3). (W) Quantification of the % tdTomato$^+$ cells that express SST in the lateral cortex at P0. (X) Quantification of the % tdTomato$^+$ cells in the MZ that are cC3$^+$, left bars; tdTomato$^+$/SST$^+$, middle bars; or tdTomato$^+$/SST$^-$, right bars. Data are represented as mean ± SEM. *$p < 0.05$, **$p < 0.01$, ***$p < 0.001$. Scale bars in (E) = 250 μm and (H, O, V) = 100 μm. Abbreviations: MZ (marginal zone), CP (cortical plate), IZ/SVZ (intermediate and subventricular zones).

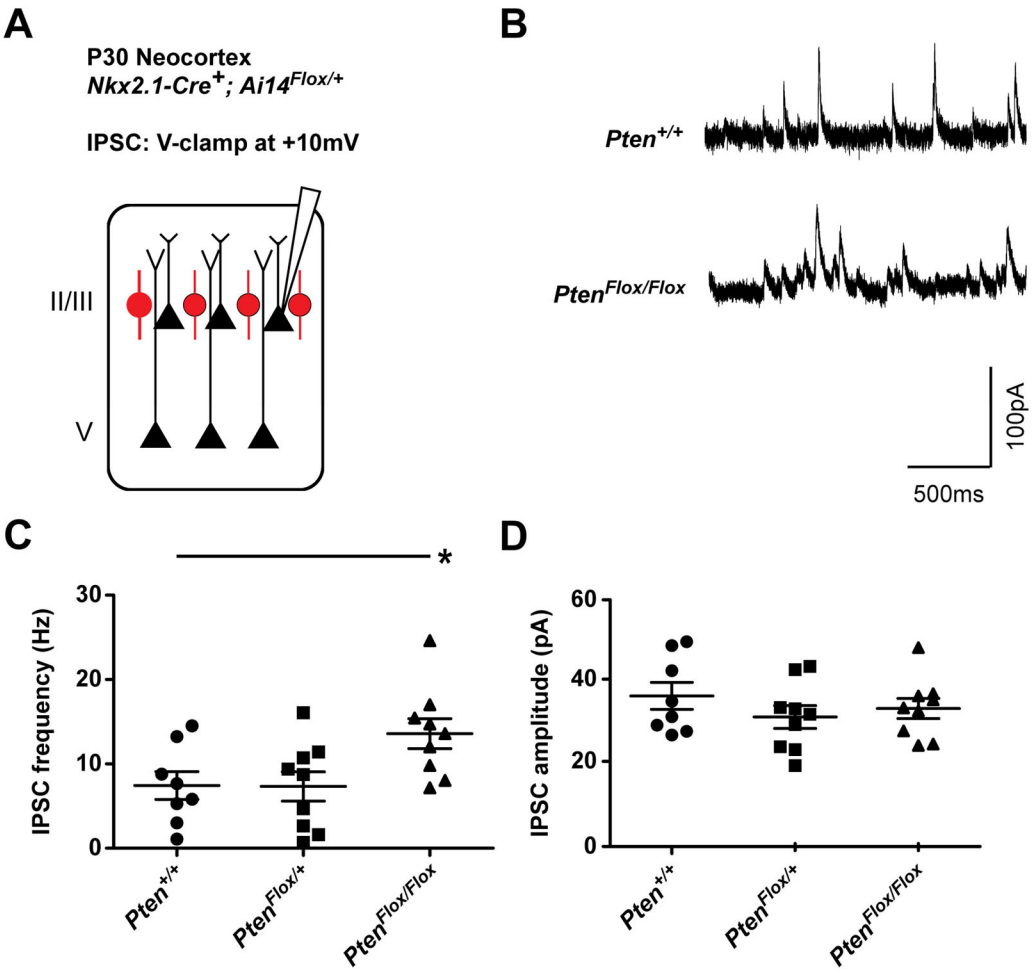

Figure 4. Neocortical principle neurons in *Nkx2.1-Cre; Pten* cKOs received increased IPSC frequency

(A) Schema of neocortical recordings performed on principle neurons in somatosensory cortical layers II/III (black) from *Nkx2.1-Cre*$^{+}$*; Ai14*$^{Flox/+}$; *Pten*$^{+/+}$, *Pten*$^{Flox/+}$ or *Pten*$^{Flox/Flox}$ slices at P30. *Nkx2.1-Cre*$^{+}$ interneurons were tdTomato^{+} (red). (B) Example traces of inhibitory postsynaptic currents (IPSCs) from *Pten*$^{+/+}$ and *Pten*$^{Flox/Flox}$ slices. Quantification of IPSC frequency onto principle neurons (C) and IPSC amplitude (D). Data are represented as mean ± SEM. *$p < 0.05$. Abbreviations: (ms) milliseconds, (Hz) hertz, (pA) picoamps.

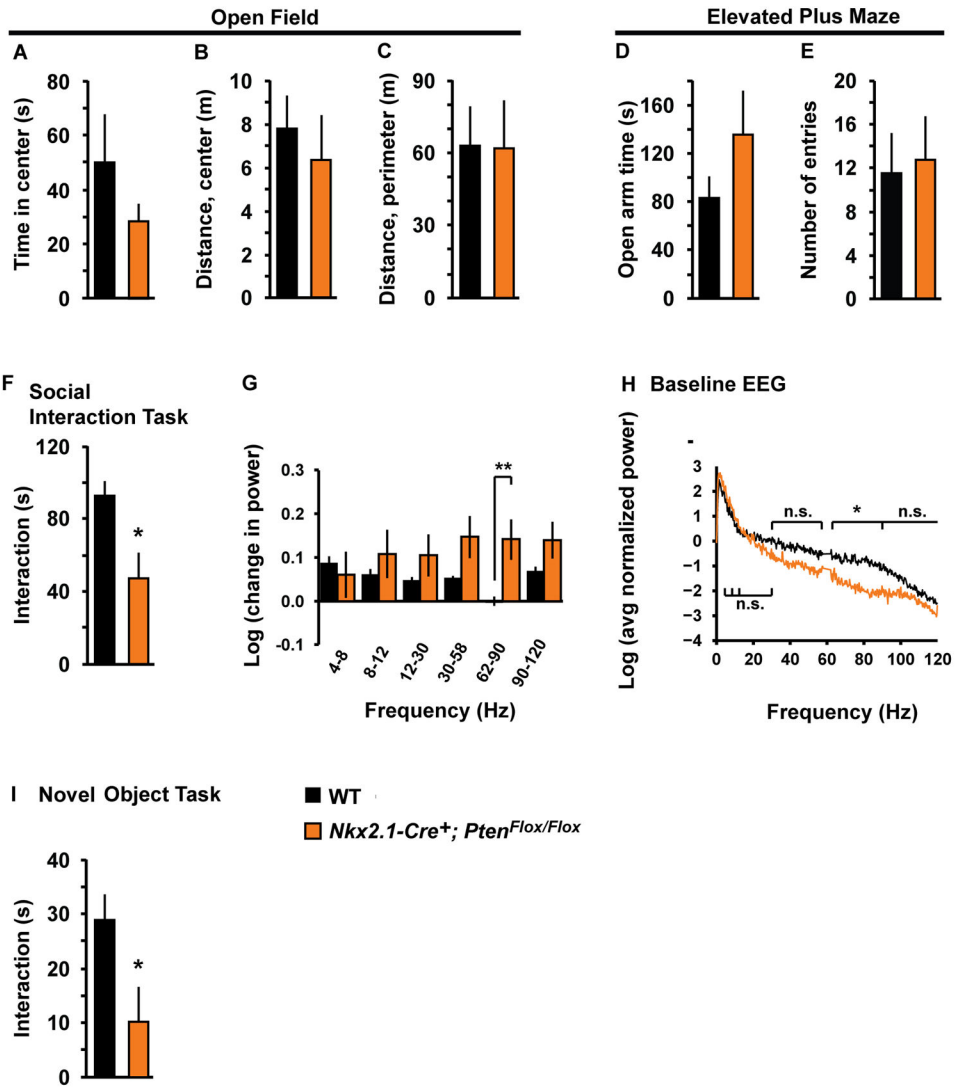

Figure 5. ***Nkx2.1-Cre; Pten*** **cKOs showed reduced social behavior and altered EEG gamma oscillations**

(A–C) Open field test: quantification of P30 *Nkx2.1-Cre*$^{+}$*; Pten*$^{+/+}$ (WT) and *Pten*$^{flox/flox}$ littermates for time spent in the center of the field (A), distance traveled in the center (B) and in the perimeter (C). (D, E) Elevated plus maze: quantification of the time spent in open arms (D) and the number of entries made (E). (F) Social interaction task: quantification of the amount of social interaction time *Nkx2.1-Cre*$^{+}$*; Pten*$^{+/+}$ (WT) and *Pten*$^{flox/flox}$ littermates spent with a stranger mouse. (G) Social interaction task: quantification of changes in electroencephalogram (EEG) power, log transformed, during periods of social interaction. Graph represents recordings made from prefrontal cortex; significant changes were in the high-γ range (62–90 Hz). (H) Prefrontal EEG, shown as the log transform of the averaged, normalized power spectrum. The graph was analyzed from a period before the social interaction test and the power spectrum from each mouse was normalized by the sum of all values from 0–120 Hz (excluding 58–62 Hz). *Nkx2.1-Cre, Pten*$^{flox/flox}$ mice exhibit a decrease in the power of prefrontal baseline high-γ (62–90 Hz) oscillations compared to

their WT littermates. (I) Novel object task: just after the social interaction assay, the time each mouse spent with a novel object was measured. (n = 5 mice per genotype, both groups). Data are represented as mean ± SEM. *$p < 0.05$, **$p < 0.01$.

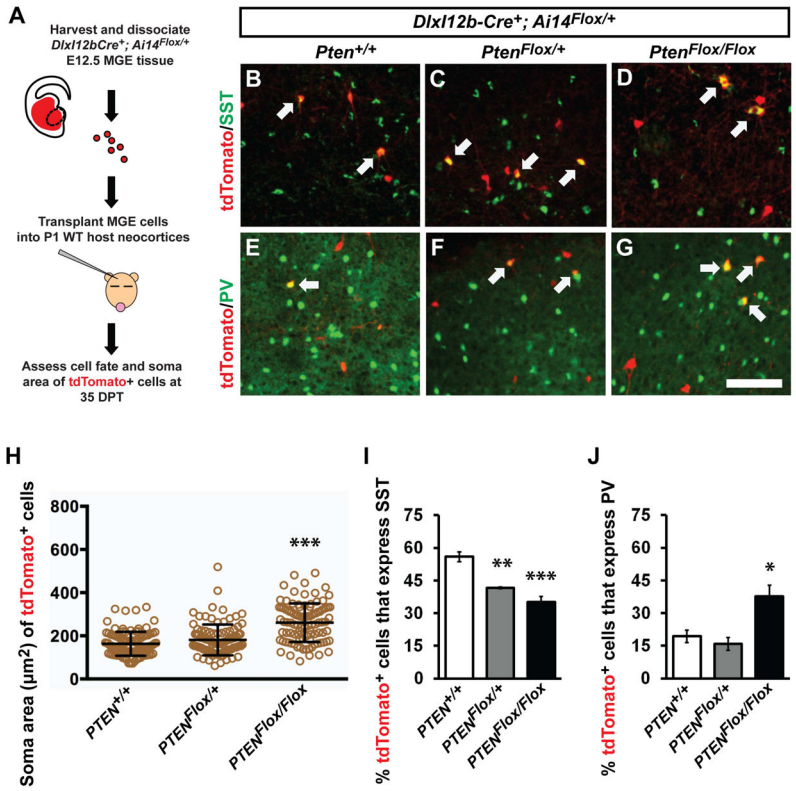

Figure 6. Cortical interneurons derived from transplanted *Pten* cKO MGE have increased soma size and increased PV^{+}/SST^{+} ratio

(A) Schema depicting the transplantation procedure. E12.5 *Dlxl12b-Cre*$^{+}$*; Ai14*$^{Flox/+}$ MGE cells (tdTomato^{+}) that were either *Pten*$^{+/+}$, *Pten*$^{Flox/+}$ or *Pten*$^{Flox/Flox}$ were transplanted into WT P1 neocortices and allowed to develop for 35 days post transplant (DPT). Coronal immunoflourescent images of neocortices transplanted with *Pten*$^{+/+}$, *Pten*$^{Flox/+}$ or *Pten*$^{Flox/Flox}$ MGE cells show coexpression of tdTomato and SST (B–D) or PV (E–G). Arrows point to coexpressing cells. Quantification of soma size of the tdTomato^{+} cells (H), and the proportion of tdTomato^{+} cells that express either SST (I) or PV (J). Data are represented as mean ± SD (H), ± SEM (I, J). (*p < 0.05, **p<0.01, ***p<0.001). Scale bar in (G) = 100 µm. **See also** Figure S4 and Table S3.

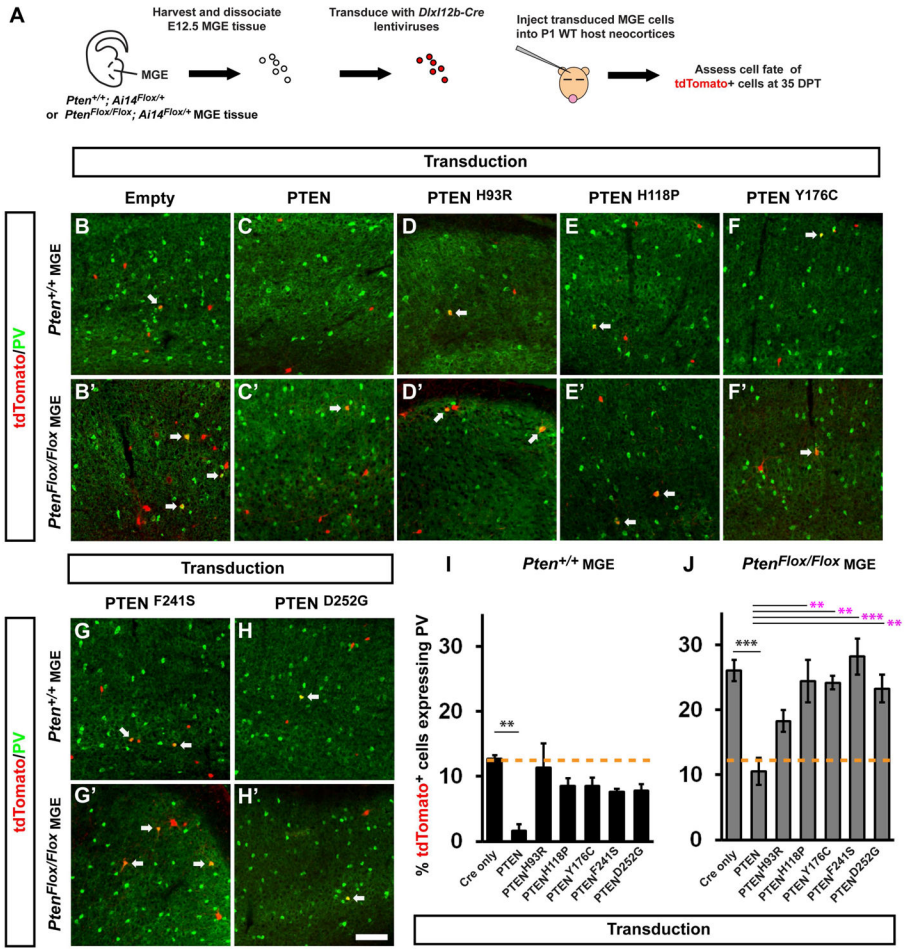

Figure 7. Complementation assay comparing WT and *PTEN* ASD alleles reveal reduced function of ASD alleles in regulating PV^{+} interneuron ratio

(A) Schema depicting the MGE transplantation and complementation assay. E12.5 control (*Pten*$^{+/+}$*; Ai14*$^{Flox/+}$) or (*Pten*$^{Flox/Flox}$*; Ai14*$^{Flox/+}$) MGE cells were transduced with a *DlxI12b-Cre-T2a-MCS* lentivirus that expresses either *Cre* only, or *Cre* with human WT *PTEN*, or a *PTEN* ASD allele, from the multiple cloning site (MCS). MGE cells were transplanted into a P1 wild type (WT) neoocortex and assessed at 35 DPT. Coronal immunoflourescent images of neocortices transplanted with transduced control (B–H) or *Pten*$^{Flox/Flox}$ (B′–H′) MGE cells show expression of tdTomato and PV at 35 DPT. Arrows point to co-expressing cells. Quantification of the % of tdTomato^{+} control (I) or *Pten*$^{Flox/Flox}$ (J) transduced-MGE cells that co-express PV. Data are represented as mean ± SEM. (n) = 4, all groups (**p<0.01, ***p<0.001, black asterisks = compared to *Cre* only lentivirus, magenta asterisks = compared to WT *PTEN* lentivirus). Scale bar in (H′) = 100 μm. **See also** Figures S5 and S6.